Available online at www.sciencedirect.com
ScienceDirect
Journal of the European Ceramic Society 30 (2010) 1815–1820
www.elsevier.com/locate/jeurceramsoc

Enhancement of the thermoelectric properties of directionally grown Bi–Ca–Co–O through Pb for Bi substitution

A. Sotelo [a,*], E. Guilmeau [b], Sh. Rasekh [a], M.A. Madre [a], S. Marinel [b], J.C. Diez [a]

[a] *ICMA (UZ-CSIC), Depto. de Ciencia y Tecnología de Materiales y Fluidos, C/María de Luna 3, E-50018 Zaragoza, Spain*
[b] *CRISMAT Laboratory, UMR 6508 CNRS-ENSICAEN, 6 Bld. Maréchal Juin, 14050 Caen cedex, France*

Received 18 August 2009; received in revised form 12 January 2010; accepted 27 January 2010
Available online 20 February 2010

Abstract

Thermoelectric performances on cobaltite ceramics can be changed by doping followed by grain orientation methods. This can be performed by the Laser Floating Zone (LFZ) method on samples with different substitutions in the Rock Salt sublattice. In this work, $Bi_{2-x}Pb_xCa_2Co_{1.7}O_y$ ($x = 0.0$, 0.2, 0.4 and 0.6) ceramics have been directionally grown at 30 mm/h. In all the cases, samples show a microstructure composed, mainly, of alternated grains of the thermoelectrical phase and the solid solution Bi(Pb)–Ca–O, with small CoO inclusions. It has been found an important improvement on the resistivity and thermopower for samples with 0.4 Pb substitution, leading to power factor values higher than usual in misfit cobaltites obtained by conventional solid state routes.

Keywords: Grain growth; Microstructure-final; Platelets; Electrical properties; Thermopower

1. Introduction

Thermoelectric (TE) materials can transform a temperature difference to electrical power directly due to the well-known Seebeck effect. This important characteristic has focused attention on this type of materials in order to be applied in waste heat recovery devices.[1]

High performance thermoelectric materials should possess large Seebeck coefficients (α), low electrical resistivity (ρ) and low thermal conductivity (κ). Low electrical resistivity is necessary to minimize Joule heating, while a low thermal conductivity helps to maintain a large temperature gradient between the hot and cold sides. The three factors, as well as absolute temperature (T), are embodied as a dimensionless factor, the Figure of Merit, zT ($\alpha^2 T/\rho\kappa$).[2]

Nowadays TE devices based on intermetallic materials with high zT values, are industrially used, e.g. in vehicles, but due to their degradation at high temperatures under air, they should not be used in devices working in those conditions. This limitation was overwhelmed by the discovery in 1997[3] of attractive thermoelectrical properties in ceramics such as $Na_2Co_2O_4$. Thus, the cobaltite ceramics have attracted attention as promising thermoelectric materials for high temperature applications. The intense research work devoted on those ceramics led to the discovery of new compositions, such as $Ca_3Co_4O_9$, $Bi_2Sr_3Co_2O_9$, $LaCoO_3$ and $Bi_2Ca_2Co_2O_y$ with high thermoelectric properties.[4–7]

Crystallographic studies on those cobaltites showed that their structure is composed of two different layers, with an alternate stacking of a common conductive CdI_2-type CoO_2 layer with a two-dimensional triangular lattice and a block layer composed of insulating rock–salt-type (RS) layers. The two sub-lattices (RS block and CdI_2-type CoO_2 layer) possess common a- and c-axis lattice parameters and β angles, but different b-axis length, causing a misfit along the b-direction.[8–10] Furthermore, the size of the RS block has an influence on the Seebeck factor.[7]

The high structural anisotropy of this type of materials leads to the formation of plate-like grains during the crystallization. This shape anisotropy opens the route to align preferentially the grains using physical, mechanical and/or chemical processes. Such grains alignment would allow attaining macroscopic properties comparable to those obtained on single crystals. Numerous methods have been reported to be efficient to obtain a good grains alignment, such as hot uniaxial pressing,[11] spark plasma sintering,[12] laser zone melting (LFZ),[13] templated grain growth

* Corresponding author. Tel.: +34 976762617; fax: +34 976761957.
E-mail address: asotelo@unizar.es (A. Sotelo).

0955-2219/$ – see front matter © 2010 Elsevier Ltd. All rights reserved.
doi:10.1016/j.jeurceramsoc.2010.01.037

(TGG),[14] *etc.* On the other hand, cation substitution in the RS layer [Gd and Y for Ca,[15] or Pb for Bi[16]] is known to improve the thermoelectric properties.

In this work, it is reported the effect of Pb for Bi substitution on the microstructure and thermoelectric properties of $Bi_{2-x}Pb_xCa_2Co_{1.7}O_y$ grown from the liquid trough the LFZ method.

2. Experimental

$Bi_{2-x}Pb_xCa_2Co_{1.7}O_y$, with $x = 0$, 0.2, 0.4 and 0.6, polycrystalline samples were prepared by the conventional solid state route using commercial Bi_2O_3 (Panreac, 98+%), $CaCO_3$ (Panreac, 98+%), Co_2O_3 (Aldrich, 98+%), and PbO (Panreac, 99+%) powders as starting materials. They were weighed in the appropriate proportions, mixed and ball milled for 30 min at 300 rpm in an agate mortar. In order to assure the total decomposition of carbonates, the mixed powders were thermally treated twice at 750 and 800 °C for 12 h under air, with an intermediate manual milling. This step is of the main importance, as it has been designed to avoid the presence of carbonates in the LFZ process, which would decompose in the melt leading to bubble formation inside the liquid phase and, more important, disturbing the crystallization front. The so obtained powders were then isostatically pressed at 200 MPa for 1 min in order to obtain green cylindrical ceramic bars, which were subsequently used as feed in a LFZ device equipped with a continuous power Nd:YAG solid sate laser (1.06 μm) and described elsewhere.[17]

The texturing processes have been performed downwards with a growth speed of 30 mm/h. In order to assure the compositional homogeneity of the molten zone and maintaining constant the textured rod diameter, the feed and the seed have been rotated at 15 and 3 rpm in opposite directions, respectively. The use of this relatively high crystallization rate implies that the growth process is not produced in an equilibrium condition. For this reason, the obtained textured cylinders are formed by the most stable phase, but accompanied by other phases (secondary phases). In spite of that multiphasic composition, the LFZ process produces long (more than 20 cm) textured cylinders, with very homogeneous diameter (in this case, ca. 2 mm). These bars were finally cut to obtain samples having the adequate dimensions for their characterization.

Powder X-ray diffraction (XRD) patterns have been systematically recorded in order to identify the different phases in the thermoelectric textured materials. Data have been collected at room temperature, with 2θ ranging between 10 and 40 degrees, using a Siemens Kristalloflex diffractometer working with Kα Cu radiation.

Microstructures have been observed by scanning electron microscopy JEOL 6000 equipped with an energy dispersive spectroscopy (EDS) device. Micrographs of longitudinal fractured sections have been recorded to observe the general grain orientation, while longitudinal polished sections of the samples have been observed to analyze the different phases and their distribution. From these pictures, an estimation of the grain misalignment from the bar axis, as well as the amount of the different phases, have been performed using Digital Micrograph software. Electrical resistivity (ρ) and Seebeck coefficient (α) or Thermopower (TEP) were simultaneously determined by the standard dc four-probe technique in a ZEM-3 measurement system (Ulvac-Riko), in the steady state mode and at temperatures ranging from 50 to 650 °C under He atmosphere. With the electrical resistivity and thermopower data, the power Factor (PF) has been calculated ($PF = \alpha^2/\rho$) in order to determine the samples performances. These electrical properties have been compared with the results reported in the literature at low temperature (~50 °C), where oxygen diffusion is negligible, to avoid the influence of the atmosphere on the compared values.

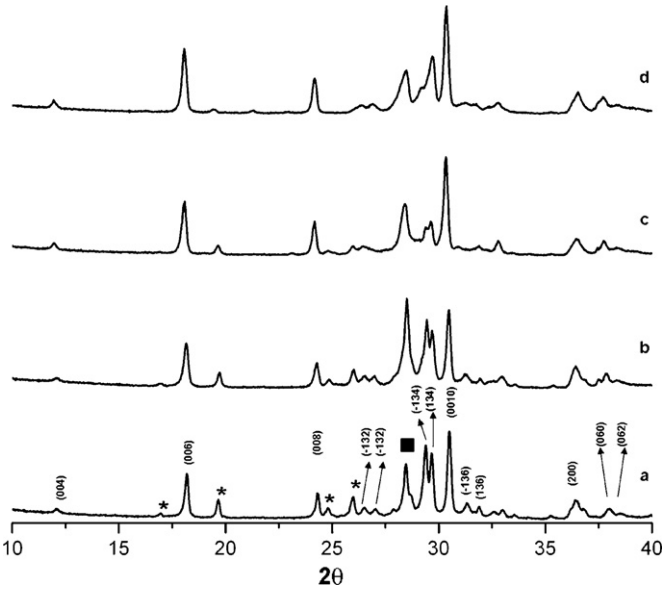

Fig. 1. Powder X-ray diffraction patterns obtained for the $Bi_{2-x}Pb_xCa_2Co_{1.7}O_x$ samples; $x = 0$ (a); $x = 0.2$ (b); $x = 0.4$ (c); and $x = 0.6$ (d). Non-thermoelectrical secondary phases peaks are indicated by an *. The ■ shows the Si (1 1 1) diffraction peak, used as reference.

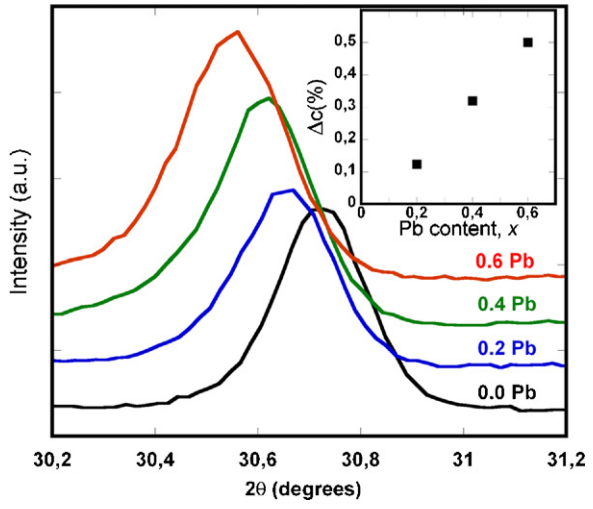

Fig. 2. Enlarged view of the (0 0 1 0) diffraction peaks of $Bi_{2-x}Pb_xCa_2Co_{1.7}O_x$ samples for $x = 0.0$; 0.2; 0.4 and 0.6, showing their displacement as a function of Pb content. The insert illustrates the relative *c*-axis variation with respect to the undoped samples.

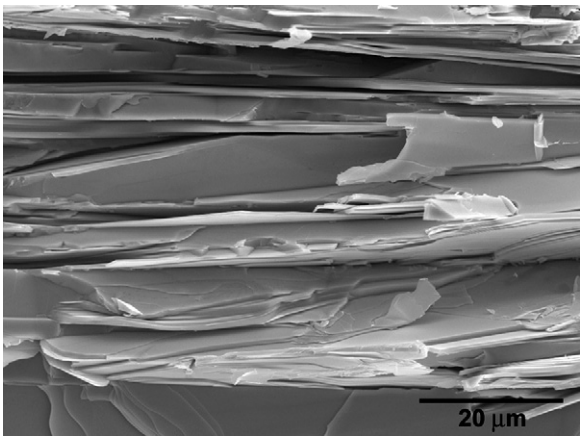

Fig. 3. SEM micrograph of a fractured $Bi_{1.8}Pb_{0.2}Ca_2Co_{1.7}O_x$ sample, showing the alignment and stacking of the plate-like grains.

3. Results and discussion

Powder XRD patterns for the different $Bi_{2-x}Pb_xCa_2Co_{1.7}O_y$ samples, grown by the LFZ process, are displayed in Fig. 1. From these data, it is clear that all the samples have very similar diffraction patterns and show minor peaks corresponding to non-thermoelectrical secondary phases. The highest peaks belong to the misfit cobaltite phase and are in agreement with previously reported data.[18] Weak diffraction peaks (marked with an *) are related to the solid solution Bi(Pb)-Ca-O secondary phases, and the ■ indicates the Si (1 1 1) diffraction peak, used as reference. Otherwise, the cobaltite peaks show a displacement towards lower angles when Pb for Bi substitution is increased, as it is illustrated in Fig. 2, due to the modification of the RS cell parameters. From the (0 0 1 0) diffraction peaks, the *c* parameter evolution has been evaluated as a function of the Pb content and it is represented in the insert of Fig. 2. A linear relationship, between the nominal Pb addition and the *c* parameter is clearly evidenced, which indicates a proportional increase of the Pb content in the TE phase. On the textured samples, which have been fractured (see Fig. 3), it is observed that each macroscopic grain is in fact composed of many, well stacked and very thin, plate-like grains (∼0.4 μm) with a large surface area (more than $60 \times 60\ \mu m^2$).

SEM micrographs overviews performed on polished longitudinal sections, displayed in Fig. 4, show that all samples are free of porosity. It can also be seen that the amount of secondary phases (observed in this figure, principally, as black contrast) decreases from 0.0 to 0.4 Pb substitution while increasing Pb substitution to 0.6 starts to increase the secondary phases content. On the other hand, grain alignment follows similar evolution; it is increased from 0.0 to 0.4 Pb content, and starts to decrease with higher Pb content. This evolution is clearly illustrated with Fig. 5, where higher magnification SEM micrographs are displayed. In this figure, it is also possible distinguish between two gray contrasts and two different black phases by their morphology. The composition of these four different phases has been determined by EDX. The different phases have been identified as: dark grey phase, corresponding to the misfit cobaltite structure, light grey phase, Co-free secondary phase and identified as a Bi(Pb)–Ca–O solid solution. The black phases can be distinguish by their aspect, the black dendritic-like phase

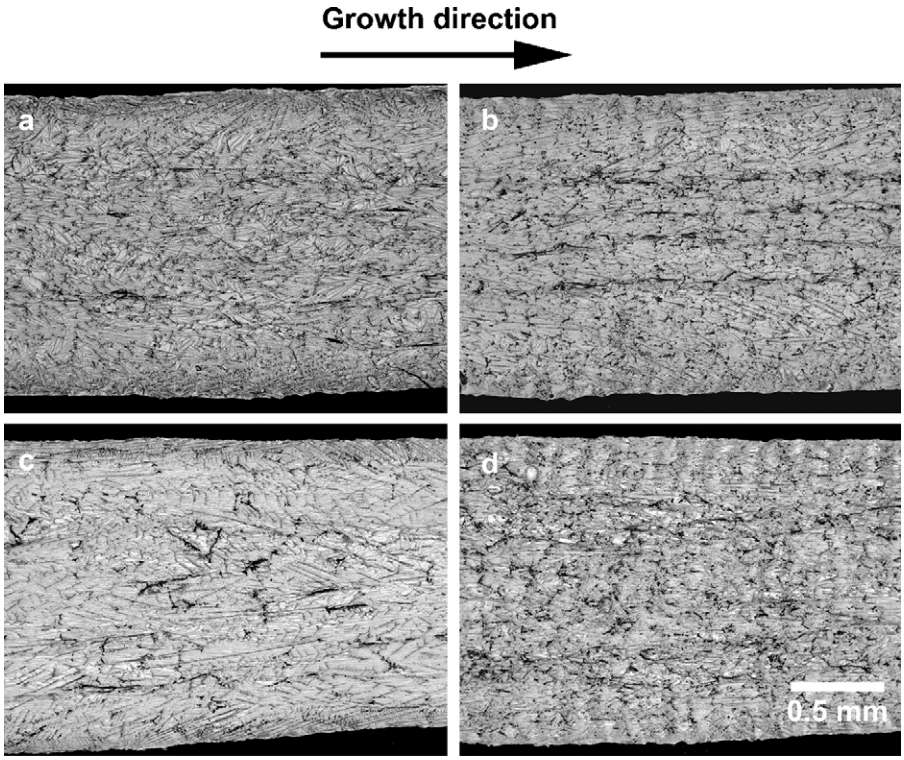

Fig. 4. General SEM micrographs of longitudinal polished sections of the $Bi_{2-x}Pb_xCa_2Co_{1.7}O_x$ samples, for $x = 0.0$ (a); $x = 0.2$ (b); $x = 0.4$ (c); and $x = 0.6$ (d). The arrow indicates the growth direction.

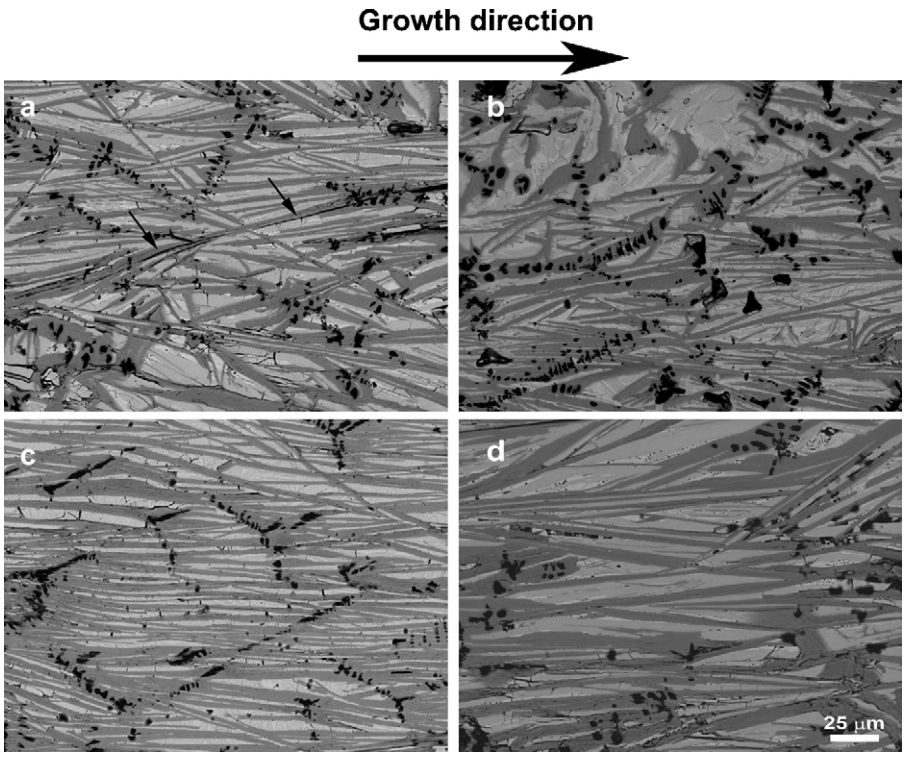

Fig. 5. Close view SEM micrographs of longitudinal polished sections of the $Bi_{2-x}Pb_xCa_2Co_{1.7}O_x$ samples, for $x = 0.0$ (a); $x = 0.2$ (b); $x = 0.4$ (c); and $x = 0.6$ (d). The upper arrow indicates the growth direction, and the small ones, the Ca–Co–O phase.

corresponding to CoO, and the very thin black plate-like phase to Ca–Co–O. This last phase is only found in Pb-free samples, and it is indicated by small arrows in Fig. 5a. In order to quantify the misalignment angle of the TE phase with the bar axis (growth direction), several SEM micrographs, have been used to determine the mean angles for the different Pb contents. These values have been determined as 13°, 10°, 6°, and 10° for Pb contents of 0.0, 0.2, 0.4 and 0.6, respectively. From those images, the amount of the TE phase has also been evaluated, obtaining mean values of, approximately, 55, 60, 70, and 55% for samples from 0.0 to 0.6 Pb, respectively.

The temperature (T) dependence of the resistivity (ρ), as a function of the Pb content of the textured materials, is shown in Fig. 6. The ρ (T) curves show a decrease of the resistivity from 0.0 to 0.4 Pb substitution, which can be related to the improvement in the TE grain orientation, as well as to the increase on the TE phase content. On the other hand, further Pb addition increases the amount of secondary phases and the misalignment of the TE phase (as indicated previously). As a consequence, the minimum values for the resistivity are obtained for samples with 0.4 Pb (about 33 mΩ cm at room temperature), which are about 50% lower than the lowest resistivity values reported for the sintered specimens[8,10] (around 80–100 mΩ cm). Moreover, it has been found for Pb substituted samples that resistivities are nearly temperature independent in the temperature range investigated. This behaviour can be explained by the Pb substitution effect on the TE phase.[19]

Fig. 7 shows the variation of the Seebeck coefficient with the temperature, as a function of the Pb content. It can be clearly seen that the sign of the thermopower is positive for the entire measured temperature range, which confirms a conduction governed by holes. The values of the thermopower increase with the temperature, with the same behaviour for all the samples and decreasing with Pb content. At about 50 °C, α values decrease from around 220 μV/K obtained for the undoped samples, to around 140 μV/K for the 0.6 Pb one. These values are, in most of the cases, higher than those reported for sintered

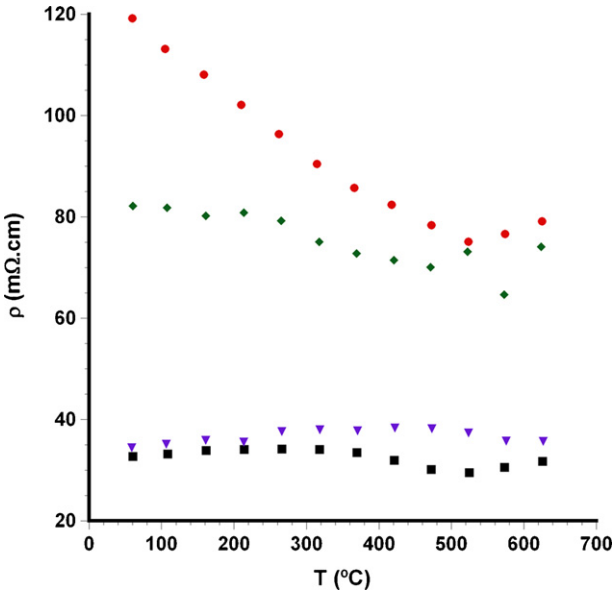

Fig. 6. Temperature dependence of the electrical resistivity, ρ, as a function of Pb content in $Bi_{2-x}Pb_xCa_2Co_{1.7}O_x$ samples, for $x = 0.0$ (●); $x = 0.2$ (♦); $x = 0.4$ (■); and $x = 0.6$ (▼).

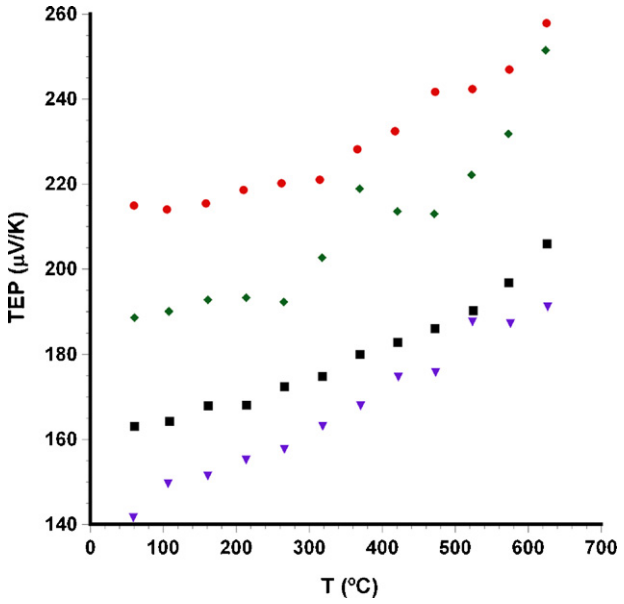

Fig. 7. Temperature dependence of the thermopower, or Seebeck coefficient, S, as a function of Pb content in $Bi_{2-x}Pb_xCa_2Co1.7O_x$ samples, for $x = 0.0$ (●); $x = 0.2$ (♦); 0.4 (■); and $x = 0.6$ (▼).

materials (usually around 150 μV/K).[7] The high value of the thermopower (until about 50% higher than those obtained for materials prepared by a conventional solid state reaction) is not common in this system, but we can give an explanation to this phenomenon: the LFZ growth can probably generate oxygen vacancies in a larger content than in bulk samples conventionally synthesised and hence, the holes concentration is, consequently, decreased due to the reduction of Co^{4+} to Co^{3+}. It has already been evidenced that, under reduced conditions, the misfit phase $[Ca_2CoO_3][CoO_2]_{1.62}$ (close to the present misfit system) contains considerable amounts of oxygen vacancies.[20]

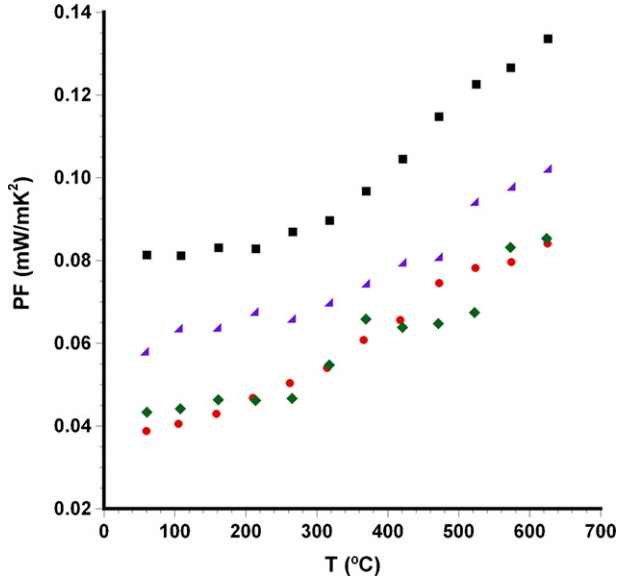

Fig. 8. Temperature dependence of the Power Factor, S^2/ρ, as a function of Pb content in $Bi_{2-x}Pb_xCa_2Co_{1.7}O_x$ samples, for $x = 0.0$ (●); $x = 0.2$ (♦); $x = 0.4$ (■); and 0.6 (▼).

In order to evaluate the thermoelectric performances of these materials, the power factor, S^2/ρ, has been calculated. The temperature dependence of the power factor (PF), estimated from the data represented in Figs. 6 and 7 is plotted in Fig. 8. When considering PF values at around 50 °C (∼room temperature), it can be clearly seen that undoped samples, as well as 0.2 Pb doped ones, have the same values (around 0.04 mW/K^2 m), followed by an impressive increase for the 0.4 Pb doped samples, reaching 0.08 mW/K^2 m, and decreasing for further Pb addition to 0.06 mW/K^2 m. These values are, in all cases higher than those obtained for the sintered specimens reported in the literature (about 0.03 mW/K^2 m at RT).

4. Conclusions

This paper demonstrates that bulk $Bi_{2-x}Pb_xCa_2Co_{1.7}O_y$ thermoelectric materials can be directionally grown by the laser floating zone method (LFZ). This process leads to a multilayer cobaltite with small compositional differences between layers, mainly in Co content. It has been found a significant decrease of the thermopower values for samples with Pb doping, while a remarkable decrease on the resistivity has been obtained.

The optimal Pb for Bi substitution has been determined using the values of the power factor at 50 °C, which is maximum for the 0.4 Pb doped samples with values around 0.08 mW/K^2 m (nearly three times higher than those reported in the literature for sintered specimens).

Acknowledgements

The authors wish to thank the Gobierno de Aragón (Research Groups T12 and T74, and project PI154/08), the Spanish Ministry for Education and Science (Spanish–French Integrated Action HF2006-0171), and the Spanish Ministry of Science and Innovation (Project MAT2008-00429) for financial support. The technical contributions of C. Estepa, J. A. Gómez and C. Gallego are also acknowledged.

References

1. Mahan G, Sales B, Sharp J. Thermoelectric materials: new approaches to an old problem. *Phys Today* 1997;**50**:42–7.
2. Rowe DM. In: Rowe DM, editor. *Thermoelectrics handbook: macro to nano*. 1st ed. Boca Raton, FL: CRC Press; 2006. p. 1-3–1-7.
3. Terasaki I, Sasago Y, Uchinokura K. Large thermoelectric power in $NaCo_2O_4$ single crystals. *Phys Rev B* 1997;**56**:12685–7.
4. Funahashi R, Matsubara I, Ikuta H, Takeuchi T, Mizutani U, Sodeoka S. An oxide single crystal with high thermoelectric performance in air. *Jpn J Appl Phys* 2000;**39**:L1127–9.
5. Masset AC, Michel C, Maignan A, Hervieu M, Toulemonde O, Studer F, Raveau B, Hejtmanek J. Misfit-layered cobaltite with an anisotropic giant magnetoresistance: $Ca_3Co_4O_9$. *Phys Rev B* 2000;**62**:166–75.
6. Leligny H, Grebille D, Perez O, Masset AC, Hervieu M, Raveau B. A five-dimensional structural investigation of the misfit layer compound $[Bi_{0.87}SrO_2]_2[CoO_2]_{1.82}$. *Acta Cryst B* 2000;**56**:173–82.
7. Maignan A, Pelloquin D, Hébert S, Klein Y, Hervieu M. Thermoelectric power in misfit cobaltites ceramics: optimization by chemical substitutions. *Bol Soc Esp Ceram V* 2006;**45**:122–5.

8. Maignan A, Hébert S, Hervieu M, Michel C, Pelloquin D, Khomskii D. Magnetoresistance and magnetothermopower properties of Bi/Ca/Co/O and Bi(Pb)/Ca/Co/O misfit layer cobaltites. *J Phys: Condens Matter* 2003;**15**:2711–23.
9. Itahara H, Xia C, Sugiyama J, Tani T. Fabrication of textured thermoelectric layered cobaltites with various rock salt-type layers by using *b*-$Co(OH)_2$ platelets as reactive templates. *J Mater Chem* 2004;**14**:61–6.
10. Guilmeau E, Mikami M, Funahashi R, Chateigner D. Synthesis and thermoelectric properties of $Bi_{2.5}Ca_{2.5}Co_2O_x$ layered cobaltites. *J Mater Res* 2005;**20**:1002–8.
11. Garnier V, Caillard R, Sotelo A, Desgardin G. Relationship among synthesis, microstructure and properties in sinter-forged Bi-2212 ceramics. *Physica C* 1999;**319**:197–208.
12. Zhang Y, Zhang J, Lu Q. Synthesis of highly textured $Ca_3Co_4O_9$ ceramics by spark plasma sintering. *Ceram Int* 2007;**33**:1305–8.
13. Sotelo A, Guilmeau E, Madre MA, Marinel S, Lemonnier S, Diez JC. $Bi_2Ca_2Co_{1.7}O_x$ thermoelectric ceramics textured by laser floating zone method. *Bol Soc Esp Ceram V* 2008;**47**:225–8.
14. Seabaugh MM, Kerscht IH, Messing CL. Texture development by templated grain growth in liquid-phase-sintered alpha-alumina. *J Am Ceram Soc* 1997;**80**:1181–8.
15. Liu HQ, Zhao XB, Zhu TJ, Song Y, Wang FP. Thermoelectric properties of Gd, Y co-doped $Ca_3Co_4O_{9+\delta}$. *Current Appl Phys* 2009;**9**: 409–13.
16. Itoh T, Terasaki I. Thermoelectric properties of $Bi_{2.3-x}Pb_xSr_{2.6}Co_2O_y$ single crystals. *Jpn J Appl Phys* 2000;**39**:6658–60.
17. Fuente GF, de la, Diez JC, Angurel LA, Peña JI, Sotelo A, Navarro R. Wavelength dependance in laser floating zone processing. A case study with Bi–Sr–Ca–Cu–O superconductors. *Adv Mater* 1995;**7**: 853–6.
18. Guilmeau E, Pollet M, Grebille D, Chateigner D, Vertruyen B, Cloots R, Funahashi R, Ouladiaff B. Neutron diffraction texture analysis and thermoelectric properties of BiCaCoO misfit compounds. *Mater Res Bull* 2008;**43**:394–400.
19. Yamamoto T, Uchinokura K, Tsukada I. Physical properties of the misfit-layered Bi,Pb–Sr–Co–O system: effect of hole doping into a triangular lattice formed by low-spin Co ions. *Phys Rev B* 2002;**65**: 184434.
20. Karppinen M, Fjellvåg H, Konno T, Morita Y, Motohashi T, Yamauchi H. Evidence for oxygen vacancies in misfit-layered calcium cobalt oxide, [CoCaO]CoO. *Chem Mater* 2004;**16**:2790–3.